JOURNAL OF RHEOLOGY

Large amplitude oscillatory shear and Fourier transform rheology analysis of branched polymer melts

D. M. Hoyle, D. Auhl, O. G. Harlen, V. C. Barroso, M. Wilhelm, and T. C. B. McLeish

Citation: Journal of Rheology (1978-present) **58**, 969 (2014); doi: 10.1122/1.4881467
View online: http://dx.doi.org/10.1122/1.4881467
View Table of Contents: http://scitation.aip.org/content/sor/journal/jor2/58/4?ver=pdfcov
Published by the The Society of Rheology

Large amplitude oscillatory shear and Fourier transform rheology analysis of branched polymer melts

D. M. Hoyle[a)]

Department of Physics, University of Durham, Durham DH1 3LE, United Kingdom

D. Auhl

Interdisciplinary Research Centre (IRC) for Polymer Science and Technology, University of Leeds, Leeds LS2 9JT, United Kingdom and Faculty of Humanities and Sciences, Maastricht University, P.O. Box 616, 6200 MD Maastricht, The Netherlands

O. G. Harlen

Department of Applied Mathematics, University of Leeds, Leeds LS2 9JT, United Kingdom

V. C. Barroso and M. Wilhelm

Institute of Chemical Technology and Polymer Chemistry, Karlsruhe Institute of Technology (KIT), Engesserstrasse 18, 76131 Karlsruhe, Germany

T. C. B. McLeish

Departments of Physics and Chemistry, University of Durham, Durham DH1 3LE, United Kingdom

(Received 21 February 2014; final revision received 20 May 2014; published 9 June 2014)

Synopsis

In this paper, the predictions of the Pompom constitutive model in medium and large amplitude oscillatory shear (LAOS) are examined using Fourier transform rheology (FTR). FTR is commonly used in combination with small amplitude oscillatory shear to fit linear Maxwell parameters to dynamic moduli, and in this paper, this process is expanded to larger strain amplitudes and to further terms in the Fourier series. For both small and large amplitudes, these higher harmonics are dependent on the nonlinear Pompom parameters and the Pompom parameter space is explored to see how experimental oscillatory shear data can infer molecular detail. In the regime of small and medium strain amplitude, there exists an asymptotic solution to the Pompom equations which depends only on the ratio of the orientation and stretch relaxation times, τ_b and τ_s. This asymptotic

[a)]Author to whom correspondence should be addressed; electronic mail: d.m.hoyle@durham.ac.uk

solution is found to be accurate up to strains of order unity and the branching priority, q, only affects the stress response at larger strains. The Pompom parameters fitted to extensional data are compared to LAOS data for three materials; two lightly branched metallocene catalyzed high density polyethylenes and a densely branched low density polyethylenes. In general, the Pompom model performs well in LAOS but tends to over predict experimental results at high strain amplitudes. © *2014 The Society of Rheology*. [http://dx.doi.org/10.1122/1.4881467]

I. INTRODUCTION

An existing challenge in linking molecular architecture to rheological measurements is to fit the free parameters of a constitutive theory to a geometrically and practically simple experiment, so that the material can then be modeled in more general complex flow situations. Such flows will typically contain a mix of shear and extensional flow, and it is necessary to simultaneously characterize both flow types. In particular, the degree of strain hardening seen in extensional flow is highly sensitive to long chain branching (LCB) and makes extensional flow a good choice for fitting constitutive theories, such as the Pompom model [Münstedt *et al.* (1998); Inkson *et al.* (1999); Malmberg *et al.* (2002)].

Various techniques have been developed using linear shear rheology to distinguish between linear and branched topologies. Gabriel *et al.* (1998) showed creep experiments can be used to distinguish between a linear low density polyethylene and a low density polyethylene (LDPE). Various authors have used small amplitude oscillatory shear (SAOS) with Cole-Cole [Vega *et al.* (1998, 1999)] and van Gurp-Palmen plots [Wood-Adams and Dealy (2000); Wood-Adams *et al.* (2000); Trinkle and Friedrich (2001); Trinkle *et al.* (2002); Lohse *et al.* (2002)]. The van Gurp-Palmen plot not only distinguishes between linear and branched polymers but also indicates the degree of LCB, although this can be masked by polydispersity [Vega *et al.* (1999); Trinkle *et al.* (2002); Wood-Adams and Dealy (2000)]. Malmberg *et al.* (2002) used SAOS and uniaxial extension to examine the amount of LCB in metallocene catalyzed polyethylenes. They found that while van Gurp-Palmen analysis of the samples detected LCB, uniaxial extension was a more sensitive technique for detecting the amount and distribution of LCB.

To investigate the nonlinear shear response several transient flow types can be modeled. Inkson *et al.* (1999) fitted Pompom spectra to extensional data and showed this gave good agreement with transient shear data. Graham *et al.* (2001) showed that a Pompom model fitted to extensional data of LDPE successfully predicts the stress development in exponential shear. However, when the procedure is reversed and the Pompom model is fitted to exponential shear, there is no guarantee of being able to capture the level of strain hardening in extensional flow. In Hoyle *et al.* (2009), it was shown that step strain measurements of polyethylenes are sensitive to the level of branching and can be predicted from Pompom spectra obtained from extensional data.

The three shear flows above (step strain, constant strain-rate, and exponential strain-rate) are all modeled well by fitting a Pompom theory to extensional data, but the converse is not true. These transient shear flows are less sensitive than extensional flow to details of the branching structure, and thus they are not as useful for characterizing constitutive theories.

Much attention has recently been focused on large amplitude oscillatory shear (LAOS) [for example, cf. the review paper: Hyun *et al.* (2011)], which explores oscillatory shear experiments for a given frequency and varying strain amplitudes, typically ranging from $\gamma_0 = 0.1$ to 4. In particular, results have been explored using Fourier transform rheology (FTR) for polymer melts, where the stress response is analyzed in Fourier space.

We wish to analyze the performance of the Pompom model in LAOS and in particular we ask if Pompom parameters derived from extensional rheology capture experimental observations in LAOS, while utilizing FTR analysis?

A. General oscillatory shear

In this study, we compare steady state oscillatory shear flow to transient shear and transient extensional flow. For a general oscillatory flow, the deformation-rate tensor $\underline{\underline{K}}$ reduces to

$$K_{xy} = \dot{\gamma} = \gamma_0 \omega \cos(\omega t), \tag{1.1}$$

where γ_0 is the strain amplitude and ω is the angular frequency of oscillation.

We can express the stress, in the quasisteady state, as its Fourier decomposition,

$$\sigma_{xy}^{FT} = \sum_{N}^{\infty} I'_N \sin(N\omega t) + \sum_{N}^{\infty} I''_N \cos(N\omega t), \tag{1.2}$$

where the Fourier coefficients, I'_N and I''_N are given by

$$I'_N = \frac{\omega}{\pi} \int_{-\frac{\pi}{\omega}}^{\frac{\pi}{\omega}} \sigma_{xy} \sin(N\omega t) dt, \tag{1.3}$$

and

$$I''_N = \frac{\omega}{\pi} \int_{-\frac{\pi}{\omega}}^{\frac{\pi}{\omega}} \sigma_{xy} \cos(N\omega t) dt. \tag{1.4}$$

The Fourier coefficients can be defined in terms of nonlinear storage and loss moduli by

$$I'_N = \gamma_0 G'_N \quad \text{and} \quad I''_N = \gamma_0 G''_N, \tag{1.5}$$

where in the limit $\gamma_0 \to 0$, G'_1 and G''_1 become the usual complex moduli in the linear regime.

We can also define the phase angle of each Fourier mode, N, as

$$\tan(\phi_N) = \frac{G''_N}{G'_N}, \tag{1.6}$$

and is commonly investigated in linear rheology for the first mode, $N = 1$ [e.g., Vittorias and Wilhelm (2007)].

Oscillatory shear flow of a fluid with characteristic relaxation time, $\bar{\tau}$, can be described using both a Deborah number and Weissenberg number which are defined as

$$De = \omega \bar{\tau} \tag{1.7}$$

$$Wi = \gamma_0 \omega \bar{\tau}, \tag{1.8}$$

where for a material described by a multimode linear Maxwell (and hence Pompom) spectra, $\bar{\tau} = \frac{\Sigma_i G_i \tau_i^2}{\Sigma_i G_i \tau_i}$.

It has been suggested that FTR is sensitive to differing levels of branching [e.g., Hyun *et al.* (2006); Hyun *et al.* (2007); Hyun and Wilhelm (2009); Kempf *et al.* (2013)] and has the advantage that LAOS is easier experimentally than extensional flow. Typically, measured quantities include the real and imaginary odd harmonics, I'_N and I''_N, where $N = 1, 3, 5\ldots$. From these parameters, the absolute value of each harmonic is examined as a fraction of the absolute first harmonic and can be defined as

$$I_{N/1} = \sqrt{\frac{I'^2_N + I''^2_N}{I'^2_1 + I''^2_1}}. \tag{1.9}$$

MacSporran and Spiers (1984) have shown that LAOS and FTR is a sensitive technique for investigating the microscopic structure of fluids, in particular the phase shift for the third harmonic, $\Phi_3 = \phi_3 - 3\phi_1$, and the third storage and loss moduli, G'_3, G''_3, are of particular interest in characterizing a material and characterizing both viscous and elastic nonlinear rheology [Neidhöfer *et al.* (2003)]. Wilhelm *et al.* (1998) showed that applying oscillatory shear to non-Newtonian linear polymers provides a tool for investigating nonlinear response independent of material. By investigating the shear response in Fourier space, higher harmonics were used to characterize nonlinearities. Wilhelm *et al.* (1999) continued investigating at the cross over from linear to nonlinear behavior using the relative magnitude of the third harmonic, $I_{3/1}$. The authors also looked at the difference between parallel plate and coneplate geometries, suggesting that results are not independent of geometry but are equivalent up to a multiplicative factor. Wilhelm *et al.* (2000) and Wilhelm (2002) used FTR with linear polymers to characterize their rheological response with respect to their molecular weight, molecular weight distribution and topology.

Debbaut and Burhin (2002) investigate high density polyethylenes (HDPE) in various oscillatory measurements including LAOS and compare them with the Giesekus model, finding reasonable agreement between experiment and theory. Neidhöfer *et al.* (2003) used FTR with various branched polystyrene solutions. Using the phase shift of the third harmonic, Φ_3, the authors were able to distinguish between linear and star branched molecules at large amplitudes. Fleury *et al.* (2004) and Schlatter *et al.* (2005) investigated various linear and branched materials in FTR. They compared the sensitivity of FTR to linear analysis such as van Gurp-Palmen and Cole-Cole plots and showed that it was more sensitive to branching than linear analysis. The authors compare two constitutive models (Wagner [Wagner and Stephenson (1979)] and the double convected Pompom (DCPP) model [Clemeur *et al.* (2003)]) and fit the models to the data in a range of plots. One of the more interesting results shows a polar representation of the real and imaginary components of the Fourier decomposed shear stress, parameterized by strain amplitude. The authors claim the Wagner model gives a better prediction of the experimental results than the DCPP model.

Hyun *et al.* (2006, 2007) compare a range of constitutive models to strain hardening and nonstrain hardening data. The authors discuss the concepts of medium amplitude oscillatory shear (MAOS) for strain amplitudes of 0.1–1 and the "intercept" of the normalized absolute third harmonic, $I_{3/1}$, which is the value of $I_{3/1}$ at a strain amplitude of 0.01. In particular for branched materials, the authors claim that the slope of $I_{3/1}$ scales with γ_0 as $I_{3/1} \sim \gamma_0^n$, where n is less than 2, as opposed to $n = 2$ for linear molecules. The authors also measure transient extensional data in an attempt to link the level of strain hardening to the nonlinear response of FTR. They also note that a single mode Pompom model has a power law of $n = 2$ in MAOS as must any model in the limit of small but finite strain amplitude. Schlatter *et al.* (2005) show the DCPP model can successfully predict $I_{3/1}$ for a range of linear, sparsely branched and densely branched polyethylenes, and

in this paper, we show that the multimode form of the original Pompom model is equally effective.

Vittorias *et al*. (2007) combined FTR, NMR, and DCPP simulations. They examined $I_{3/1}$ and Φ_3 and extended the van Gurp-Palmen method to the third harmonic, $\Phi_3^0 = lim_{\gamma_0 \to 0}\Phi_3$, extrapolating to zero strain amplitude and investigated optimum experimental conditions for distinguishing the branching structure of various polyethylene samples. They found that the extended van Gurp-Palmen method is sensitive to LCB and found low frequencies optimized the nonlinear stress response. The data was modeled with the DCPP model, using only four modes. This model was able to predict $I_{3/1}$ and Φ_3 reasonably accurately although deviations from experimental data did exist. Vittorias and Wilhelm (2007) examined SAOS, LAOS, and FTR for linear and branched polyethylenes and showed that FTR is capable of determining the degree of LCB and that LAOS is more sensitive to LCB than SAOS. However, the authors point out that FTR still needs to be explored using well characterized polymer architectures.

Wapperom *et al*. (2005) investigated LAOS for a HDPE comparing it to the predictions of various constitutive equations, mainly focusing on the molecular stretch function (MSF) theory but also considered the Doi–Edwards, Carreau–Yasuda, and Giesekus models. They found that the MSF model over predicted the shear stress, although it fitted the phase shift well. The Doi–Edwards model gave a better prediction of the stress than the MSF model; however, the MSF model is able to capture strain hardening and only requires one parameter.

In their paper deriving DPP (a simplified form of the DCPP model) formulation of the Pompom model, Clemeur *et al*. (2003) calculated the response of the model to a double step strain and LAOS with FTR. They presented the LAOS results in the form of Lissajous plot of stress against strain. This makes nonlinear behavior apparent by observing visual distortion to the ellipse of linear response. The DPP model performs reasonably well, capturing the intensity of the harmonics and the deviations in the Lissajous plot up to strains of around five.

More recently, Hyun and Wilhelm (2009) introduced the quantities Q and Q_0, which are defined as $Q = I_{3/1}/\gamma_0^2$ and $Q_0 = lim_{\gamma_0 \to 0}Q$, respectively, where the 0 subscript denotes the limit of zero strain amplitude. The authors show that both Q and Q_0 are sensitive to molecular architecture and that Q_0 as a function of Deborah number can be explored using TTS to increase the experimental range available. Hyun *et al*. (2013) used the Q parameter to investigate a single mode Pompom model and showed how the ratio of arm and backbone molecular weights in a Pompom molecule had affected the Q parameter. This differs from this work where we investigate the Pompom dynamics in LAOS and build toward using a multimode Pompom model using experimental data to show we can infer molecular properties of a LCB melt. In other recent work, Wagner *et al*. (2011) investigated how Q_0 varies with frequency to study the difference between linear and comb architecture polystyrenes. This work used the MSF theory to discriminate between linear molecules and combs with entangled and unentangled branches.

In this work, we examine a variety of materials in SAOS and LAOS to see if these techniques can successfully distinguish between levels of branching. We will also explore the Pompom parameter space in order to understand what characterization or molecular information of a material can be obtained from LAOS.

II. THE POMPOM MODEL

Polymer rheology for highly entangled molecules can be successfully correlated with molecular topology. The concept of the tube model introduced by Edwards and de Gennes

[cf. Doi and Edwards (1986)] can be applied to branched polymers, in particular McLeish and Larson [McLeish and Larson (1998); McLeish (2002)] developed a molecular theory for the nonlinear dynamics of an entanglement melt of Pompom molecules. A Pompom consists of a backbone with an equal number of arms attached to branch points at either end. As with the tube model for linear polymers, the entanglements around the backbone are smoothed to a tube that moves affinely with the applied deformation and restricts lateral movement. However, unlike the linear case where polymers can diffuse freely along its tube, the presence of two branch points impedes motion along the tube giving a different stress response to deformation. In particular, the stretch relaxation time (which controls the triggering of extensional hardening) is much longer than for a comparable linear melt.

In extensional flows of sufficient rate to stretch the backbone, the backbone is stretched until its effective curvilinear tension matches the cumulative equilibrium tensions in the q arms, at which point the branch points retract into the elongating backbone tube. Equating the tension in the backbone with the maximum tension the arms can hold gives the supremum for the stretch to be $\lambda = q$. This parameter is called the branching priority. The stress exerted by the backbone segments is defined as the product of the square of the backbone stretch with a unitary tensor, the orientation tensor.

There have been several suggested algorithms for calculating the orientation tensor in the Pompom model. It was originally derived in integral form, then in a differential approximation based on the upper-convected Maxwell model for the central orientation structure. The differential model is more commonly used, particularly in complex flow calculations as it is computationally simpler, but it is not in quantitative agreement with the integral model [McLeish and Larson (1998)].

Other differential constitutive models were subsequently developed. A thermodynamically motivated differential model was suggested by Öttinger (2001). Verbeeten *et al.* (2001) also suggested the extended Pompom (XPP) differential model, which was the motivation for other subsequent forms such as the DCPP [Clemeur *et al.* (2003)]. These models were developed to avoid the maximum stretch condition and improve the quantitative agreement with the integral model, in particular to give a nonzero second normal stress difference in shear. In this paper, we will use the form of the multimode Pompom model derived by Inkson *et al.* (1999) with the modifications of Blackwell *et al.* (2000) and Lee *et al.* (2001).

In the multimode Pompom, the extra stress tensor is formed as the sum contributions from different relaxation modes [Inkson *et al.* (1999)]. The stress contribution from each mode is the product of the corresponding backbone stretch, $\lambda(t)$, and orientation tensor, $\underline{\underline{S}}(t)$,

$$\underline{\underline{\sigma}} = 3\sum_{i}^{N} G_i \lambda_i^2(t)\underline{\underline{S}}_i(t), \tag{2.1}$$

where G_i are the elastic moduli and i is the mode index.

The differential approximation uses the upper-convected Maxwell constitutive equation for the orientational degrees of freedom only, where the auxiliary tensor $\underline{\underline{A}}$ satisfies,

$$\frac{D\underline{\underline{A}}}{Dt} = \underline{\underline{K}} \cdot \underline{\underline{A}} + \underline{\underline{A}} \cdot \underline{\underline{K}}^T - \frac{1}{\tau_b}\left(\underline{\underline{A}} - \underline{\underline{I}}\right). \tag{2.2}$$

The orientation is given by the unit tensor,

$$\underline{\underline{S}} = \frac{\underline{\underline{A}}}{tr\underline{\underline{A}}}. \tag{2.3}$$

In the original Pompom model, the tension in the backbone is derived from a force balance between the drag force on each branching point and the backbone of the molecule acting as a Hookean spring, imposing an elastic stretch relaxing toward the equilibrium length of the backbone. Each arm has a maximum thermal tension that it can hold before it becomes entropically more favorable to withdraw the arms into the backbone tube. This gives a maximum stretch of $\lambda_i = q_i$, where q_i is the parameter specifying the effective degree of branching of mode i.

The flow induced branch point displacement discussed by Blackwell *et al.* (2000) modifies the relaxation rate for the stretch before the critical condition $\lambda_i = q_i$ is met via the physics of limited branch point withdrawal within the confining field of a tube diameter. Since the relaxation time has an exponential dependence on the length of the arms, there is a reduction in the relaxation time, $\tau_s \rightarrow \tau_s e^{-\nu^*(\lambda-1)}$, with $\nu^* = \frac{2}{q-1}$, [McLeish (2002)]. Writing the stretch as the dimensionless parameter, $\lambda(t) = (L(t)/L_0)$, gives a stretch equation which is nonlinear in $\lambda(t)$,

$$\frac{D}{Dt}\lambda(t) = \lambda(t)\underline{\underline{K}} : \underline{\underline{S}} - \frac{1}{\tau_s}(\lambda(t) - 1)e^{\nu*(\lambda_i - 1)}. \tag{2.4}$$

Lee *et al.* (2001) introduced a way of treating entangled chains in reversing flow consistent with tube model physics, whereby a change in sign of the applied strain would reduce the primitive path of the backbone chain to below that of equilibrium length, that is, $\lambda < 1$. A subsequent modification to the Pompom equations derived by Lee *et al.* (2001) accounts for this process and alters the orientation relaxation time to,

$$\frac{1}{\tau_b^*} = \frac{1}{\tau_b} + \frac{\dot{\lambda}}{\lambda} - \underline{\underline{K}} : \underline{\underline{S}} \quad \text{for } \lambda < 1. \tag{2.5}$$

This aspect of the Pompom model is clearly essential to treat LAOS flows, since these contain high-amplitude reversals of deformation repeatedly. Equations (2.1)–(2.3) (differential model) and [(2.4) and (2.5)] constitute the Pompom models employed here.

III. NUMERICAL METHODS

The stress generated in the Pompom model in oscillatory shear and its Fourier decomposition were calculated simultaneously. In shear flow, the constitutive equations for the Pompom model reduce to

$$\frac{dA_{xy}}{dt} = \dot{\gamma} - \frac{1}{\tau_b^*}A_{xy}, \tag{3.1}$$

$$\frac{dA_{xx}}{dt} = 2\dot{\gamma}A_{xy} - \frac{1}{\tau_b^*}(A_{xx} - 1), \tag{3.2}$$

$$\frac{d\lambda}{dt} = \frac{\dot{\gamma}A_{xy}}{A_{xx} + 2}\lambda - \frac{1}{\tau_s}(\lambda - 1)e^{\nu^*(\lambda-1)}. \tag{3.3}$$

The orientation equations needed to be solved numerically since the relaxation time, τ_b^*, is a function of the nonanalytic stretch function, $\lambda(t)$, in reversing flow [cf. Eq. (2.5)]. Equations (3.1)–(3.3) are solved using a fourth order Runge-Kutta scheme [Burden and Faires (2001)]. Quadruple precision was used to avoid round-off when solving solutions

at low-strain amplitude. In choosing appropriate values for the time-step, some calculations were performed using a fifth order Runge-Kutta-Fehlberg scheme [Burden and Faires (2001)] and solutions were checked for time-step independence for a large range of frequencies and strain amplitudes. At small Weissenberg numbers, the third harmonic, I_3, is of order W_i^3 making it difficult to compute accurately at very small W_i. Good convergence at both low and high strain amplitudes occurs for a step size of 10^{-3} times the period of oscillation and lower.

To further reduce numerical noise, the time-step was chosen so that the period is an integer number of steps. Convergence to steady state was checked by ensuring the maximum stress response for each period agreed to five significant figures before the start of the Fourier integral, and the Fourier transform was performed over multiple cycles to increase noise cancellation. The Fourier transform was calculated using a five point extension on the trapezoid rule, known as Bode's rule, which has an error of order $h^7 f^{(6)}$ [Press *et al.* (1996)]. Care must be taken when performing the numerical Fourier transform since an aliasing numerical artifact can appear if the number of periods sampled is not sufficiently larger than the Deborah number. This will be discussed in more detail in Sec. IV C.

The noise level of the Fourier transform was calculated from the second harmonic, which is mathematically zero for the Pompom model. For strain amplitudes larger than $\gamma_0 = 0.1$, the absolute value of the second harmonic was less than 1% of the absolute value of the third harmonic. The low-strain asymptotic solution detailed in Sec. IV removes the need to calculate the solution at very low Weissenberg numbers.

IV. THE POMPOM MODEL IN OSCILLATORY SHEAR

In this section, we examine a one mode Pompom model in oscillatory shear to outline the influence of the parameters on the predictions for LAOS. The Deborah number and the Weissenberg number are defined with respect to the orientation relaxation time as $De = \omega\tau_b$ and $W_i = \gamma_0\omega\tau_b$, respectively. The Pompom model has two additional parameters, $r = (\tau_b/\tau_s)$, the ratio of relaxation times and, q, the branching priority.

In Fig. 1, the stress response of a one mode Pompom model with various values of q and constant ratio of $(\tau_b/\tau_s) = r = 4$ are shown. The stress is plotted against time and strain (Lissajous plots) for a constant Deborah number, $De = 12$, for $q = 1$, 2, 5, and 10. At a Weissenberg number of $W_i = 1.2$ ($\gamma_0 = 0.1$), the stress response is linear and is independent of q, so all four lines superimpose. At $W_i = 12$ ($\gamma_0 = 1$), all cases with $q > 1$ still superimpose, however, for $q = 1$ the stress deviates slightly from linear behavior. For a high Weissenberg number, $W_i = 120$ ($\gamma_0 = 10$), the linear model with $q = 1$ is dramatically different from the branched models, $q > 1$. For $q = 1$, a double peak is observed which corresponds to cusps in the Lissajous plots. Similar shaped plots that have been observed in experiments [Li *et al.* (2009)] and even hysteresis loops have been shown to be evident in certain circumstances at the cusps [Ewoldt *et al.* (2008); Ewoldt and McKinley (2010)]. Even at this high-amplitude, there is a little difference in the stress response for $q > 1$, indicating that the Pompom model in LAOS is not very sensitive to the branching priority. This is confirmed in more detail using FTR later in Sec. IV A.

Figure 2 shows the same plot as Fig. 1 for constant branching priority, $q = 5$ but with the ratio of orientation and stretch relaxation times varied through $r = 1$, 2, 4, and 8. For a Deborah number $De = 12$ with increasing Weissenberg number, the stress response changes more dramatically than for the case with varied q parameter. For a Weissenberg number of $W_i = 120$, the stress response is attenuated with increasing relaxation time ratio. Thus, we conclude that for $q > 1$ the stress response of the Pompom constitutive

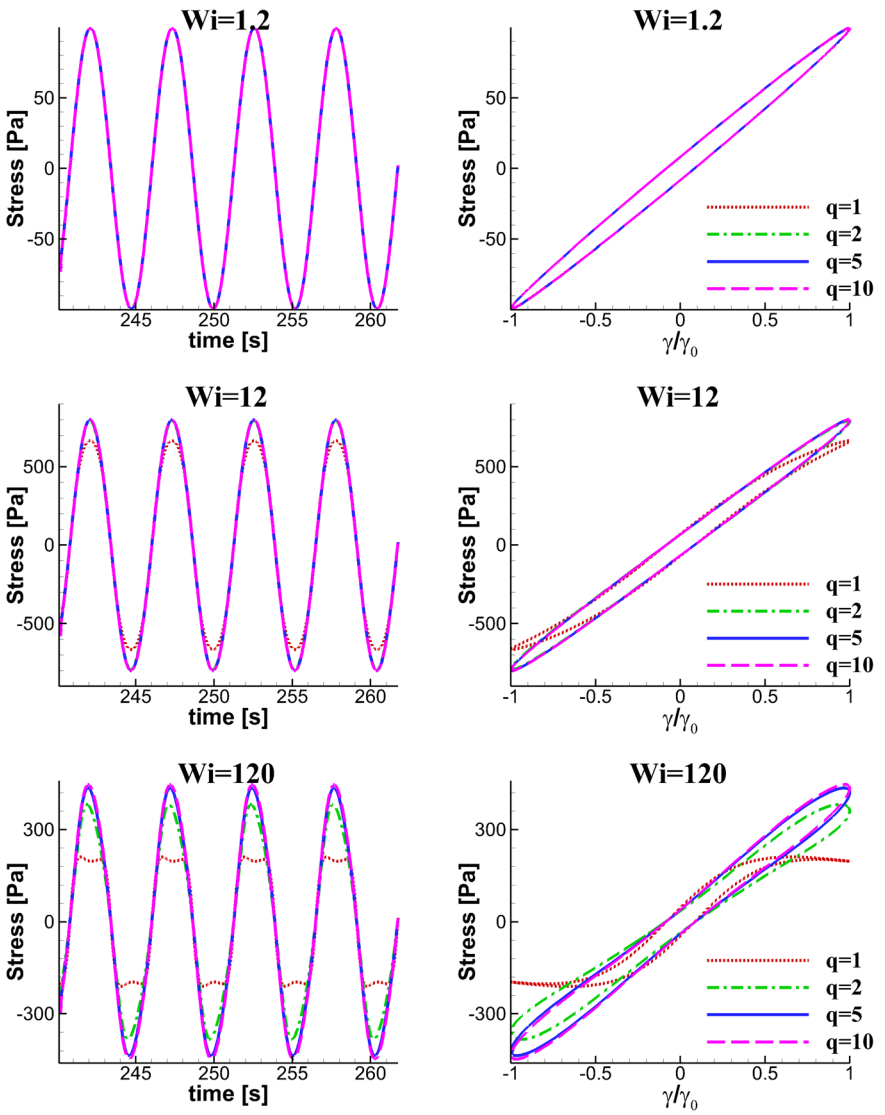

FIG. 1. A one mode Pompom model in oscillatory shear with various choices of the branching parameter, $q = 1$, 2, 5, and 10. The other Pompom parameters chosen are $G = 1000\,\text{Pa}$, $\tau_b = 10\,\text{s}$ and $r = 4$, giving a constant Deborah number for each simulation as $De = 12$. As the Weissenberg number increases the most noticeable difference is for the case $q = 1$. The stress response has low sensitivity to values of $q > 1$.

model in LAOS is more sensitive to changes in the ratio of relaxation times than to changes in branching priority.

A. Fourier transform rheology

The stress response of the Pompom model seems to be particularly sensitive to the ratio of orientation and stretch relaxation times, $r = (\tau_b/\tau_s)$. This ratio is proportional to the number of effective entanglements along the backbone. A technique that is sensitive solely to this ratio would provide a unique tool for the analysis of branched materials. To study LAOS in further detail, it becomes more convenient to examine the stress response in Fourier space rather than the time domain [Wilhelm *et al.* (1999); Wilhelm (2002)].

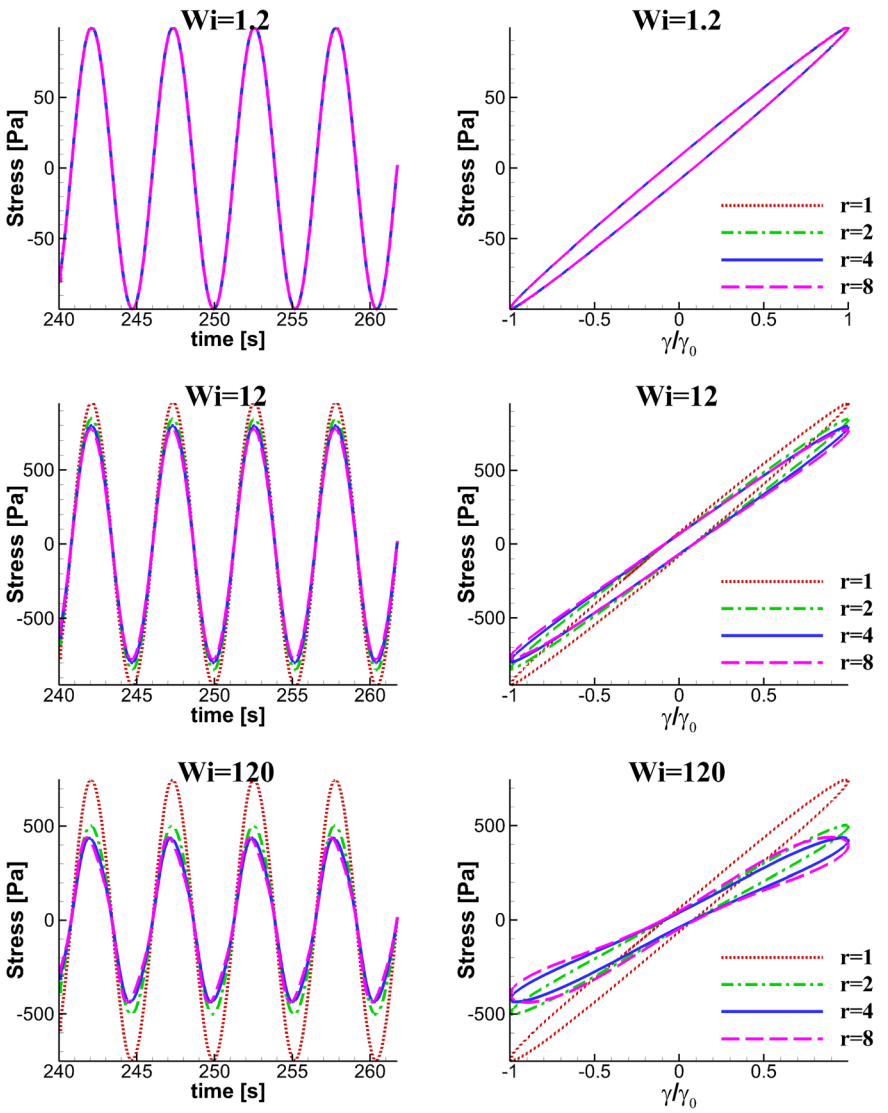

FIG. 2. A one mode Pompom model in oscillatory shear with various choices of the stretch relaxation ratio, $r = 1$, 2, 4, and 8. The other Pompom parameters chosen are $G = 1000$ Pa, $\tau_b = 10$ s and $q = 5$, giving a constant Deborah number for each simulation as $De = 12$. Compared to the branching parameter (Fig. 1) the stress response is more sensitive to variations and stretch relaxation time.

The Fourier coefficients of the harmonic series can be studied independently to find which is particularly sensitive to molecular structure. The first harmonics of the series are already commonly used in the linear regime to fit Maxwell modes for various constitutive equations including the Pompom model where they are used to determine $\{G_i, \tau_{b_i}\}$ and hence give some information about the structure of the material. We will focus on the third harmonic and examine its sensitivity to the nonlinear Pompom parameters, q and r.

B. Asymptotic solutions

A series of low-strain asymptotic solutions can be derived to achieve analytical solutions for Eqs. (1.3) and (1.4). This derivation is first shown in full in

Hoyle (2010), we review some of the results here. We can use these to look for deviations from linear behavior. Once verified, these results can also be used to reduce computation time for calculating the Fourier coefficients, as a very small time-step is required to resolve the Fourier integrals for very low-strains. A high strain asymptote for the case of $q=1$ can also be derived to examine the high strain limit of a linear Pompom model.

To derive low-strain asymptotes, it is convenient to rewrite the upper convected Maxwell (UCM) tensor as an expansion in powers of the strain amplitude, γ_0

$$\underline{\underline{A}} = \underline{\underline{I}} + \gamma_0 \underline{\underline{a}}_1 + \gamma_0^2 \underline{\underline{a}}_2 + \cdots, \tag{4.1}$$

and, similarly the stretch equation can be written as

$$\lambda(t) = 1 + \gamma_0 \lambda(t)_1 + \gamma_0^2 \lambda(t)_2 + \cdots. \tag{4.2}$$

In the case when $\tau_b^* = \tau_b$, the expansion terminates after the quadratic term. The changes to τ_b^* are negligible in the low-strain limit and can be neglected. Simulations show that changes in τ_b^* affect the Pompom stress response for strain amplitudes higher than unity. The resulting shear stress can be expanded in odd powers of γ_0. The leading order term is

$$\sigma_{xy} = \frac{G\tau_b\omega(\cos(\omega t) + \tau_b\omega\sin(\omega t))}{1+\tau_b^2\omega^2}\gamma_0 + O(\gamma_0^3). \tag{4.3}$$

Taking the Fourier transform of this result restores the familiar Maxwell storage and viscous moduli,

$$I_1' = \frac{GDe^2}{1+De^2}\gamma_0 + O(\gamma_0^3), \tag{4.4}$$

and

$$I_1'' = \frac{GDe}{1+De^2}\gamma_0 + O(\gamma_0^3), \tag{4.5}$$

where the Deborah number is given by, $De = \omega\tau_b$, and the frequency is given in rad·s^{-1}.

We can go on from the first harmonic to derive subsequent low-strain asymptotic results for higher odd harmonic results (since the even Fourier coefficients are zero identically). The leading order term in I_n' and I_n'' is of order γ_0^n for n odd and containing only odd powers of γ_0. In the limit of low-strain, only the leading power is of importance and so higher order terms can be neglected. These were calculated by hand and checked using the MAPLE symbolic algebra program. We give the result for the third harmonic and concentrate on this since the third harmonic contains the next major piece of information on nonlinearity. The storage and loss modulus for the third harmonic, in their low-strain limit are given by

$$I_3' = \frac{GDe^4(1-r^{-1})(De^2+5De^2r^{-1}-2-r^{-1})}{(1+4De^2r^{-2})(1+4De^2)(1+De^2)^2}\gamma_0^3 + O(\gamma_0^5), \tag{4.6}$$

and

$$I_3'' = -\frac{GDe^3(1-r^{-1})(4De^4r^{-1}-5De^2-8De^2r^{-1}+1)}{2(1+4De^2r^{-2})(1+4De^2)(1+De^2)^2}\gamma_0^3 + O(\gamma_0^5). \tag{4.7}$$

The two coefficients for the third harmonic are a function of Deborah number and the ratio, r, of the orientation and stretch relaxation times. Neither asymptote is dependent on the branching parameter, q, so that the influence of branching is only present in the large amplitude regime, i.e., for $Wi \gg 1$. It should be noted that the branching priority would enter asymptotic solutions of higher harmonics through the expansion of the exponential relaxation term in Eq. (3.3).

In Fig. 3, we show the variation in $I'_{3/1}$ and $I''_{3/1}$ with frequency, ω, where $I'_{3/1}$ is defined as $\left(I'_3/I_1\right)$ and similarly $I''_{3/1} = \left(I''_3/I_1\right)$. We plot the resulting $I'_{3/1}$ and $I''_{3/1}$ scaled by γ_0^2 on a linear axis, as there exists a regime of negative contribution. The frequency is still on a log axis. The modulus of the relative third harmonic [Eq. (1.9)] is also overlayed. For each modulus, $I'_{3/1}$ and $I''_{3/1}$, there exists a maximum/minimum contribution to the stress, depending on frequency.

We see in Fig. 4 that a higher ratio implies a higher maximum of $I_{3/1}$. In other words, a higher ratio implies a smaller τ_s and hence a smaller contribution to the stretch term in the extra stress. Also, the Deborah number at which the peak occurs is higher for larger ratios, r. Note, from Eqs. (4.6) and (4.7) for a ratio, $r = 1$, there is no contribution of the third harmonic to the total stress. In fact, the contribution is of order, $O(\gamma_0^5)$ and can be calculated analytically.

We also see in Fig. 4 that the case of $q = 1$ with the physical limit of $\lambda < q$, stretch relaxation is effectively instantaneous hence, $\tau_s = 0$. This causes the values I''_3 and I'_3 to have characteristically different behavior from the cases with stretch relaxation occurring. Again, from Eqs. (4.6) and (4.7), the value of $I'_{3/1}$ is the most dramatically different and is nonzero in the high frequency limit, in contrast to the case for $q > 1$. This behavior is unphysical as this model rejects chain Rouse modes. The difference between $I''_{3/1}$ for $q = 1$ and $q > 1$ occurs in the high frequency regime. For the case $q = 1$, $I''_{3/1}$ does not

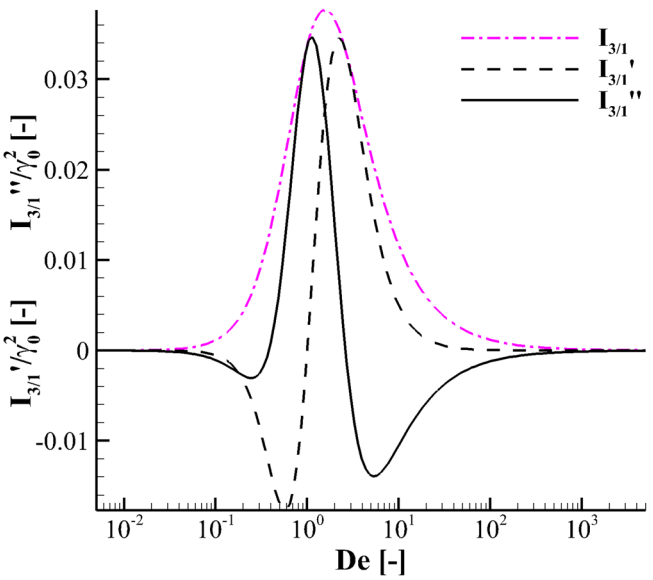

FIG. 3. A plot of $I'_{3/1}$, $I''_{3/1}$, and $I_{3/1}$ as a function of Deborah number. Parameters used were $G = 1$ Pa, $\tau_b = 1$ s, and $\tau_s = 0.25$ s.

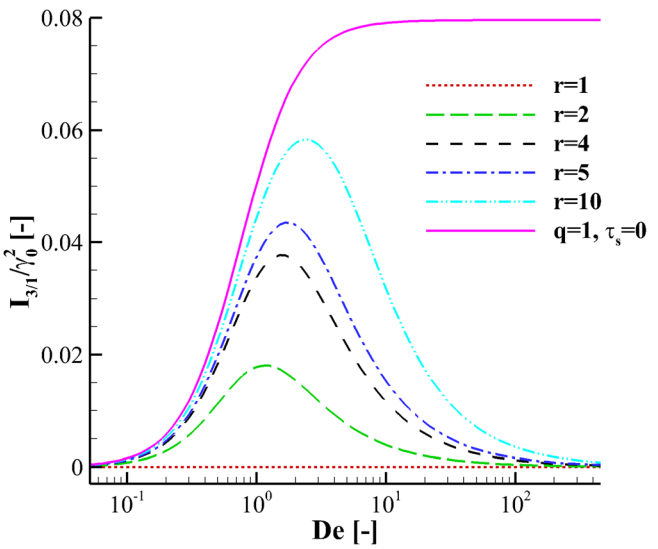

FIG. 4. A plot of $I_{3/1}$ as a function of Deborah number for various ratios, $r = 1$, 2, 4, 5, 10 and $r = \infty$. The linear parameters are $G = 1$ Pa and $\tau_b = 1$ s. The maximum in I_3 increases as a function of r up to the case of $\tau_s = 0$ s $(r = \infty)$ which has asymptotically different behavior compared to finite r.

have a second minimum as it does for the cases where $q > 1$ (cf. Fig. 3). Again, this is due to the lack of any chain stretch modes in this model.

One method for incorporating the rheology of a linear molecule is to set the stretch relaxation time to the Rouse time and allow $q \to \infty$. This limit approximates to the RoliePoly constitutive equations [Graham *et al.* (2003)] without convective constraint release and this limit has been previously studied by Venerus (2005) and Venerus and Nair (2006) to successfully model step strain flow of both finite and ideal step imposition time.

In the case of $q = 1$, we can derive high strain asymptotes for each Fourier coefficient. Using the previous expansion of the UCM tensor in powers of the strain amplitude [Eq. (4.1)], it can be shown that in high strain all Fourier coefficients scale as γ_0^{-1}. Subsequently, the Fourier coefficients for the first harmonic can be expressed as

$$I_1' = \frac{1}{\gamma_0}\frac{\sqrt{3}G\left(2De\sqrt{(3(1+4De^2))} - 4De^2 - 1\right)}{De\sqrt{(1+4De^2)}}, \tag{4.8}$$

$$I_1'' = \frac{1}{\gamma_0}\frac{3G}{De}, \tag{4.9}$$

and the Fourier coefficients for the third harmonic can similarly be written as

$$I_3' = -\frac{1}{\gamma_0}\frac{\sqrt{3}G\left(20De^4 - 6De^3\sqrt{3(4De^2+1)} - 17De^2 + 6De\sqrt{3(4De^2+1)} - 1\right)}{De(1+De^2)\sqrt{4De^2+1}}, \tag{4.10}$$

and

$$I_3'' = \frac{1}{\gamma_0}\frac{\sqrt{3}G\left(11De^2\sqrt{3(4De^2+1)} - \sqrt{3(4De^2+1)} - 36De^3\right)}{De(1+De^2)\sqrt{4De^2+1}}. \tag{4.11}$$

Unfortunately, we have not been able to find an equivalent solution for $q > 1$.

The high strain asymptote (for $q = 1$ only) is independent of strain amplitude and so for a fixed Deborah number it is also independent of Weissenberg number, as seen in Fig. 6. The value of $I_{3/1}$ has two regimes in high strain. For low Deborah numbers, $De \ll 1$, the ratio of the third and first absolute harmonics is $\sim$1, implying each harmonic contributes equally in the Fourier series. For $De \gg 1$, the value of $I_{3/1}$ plateaus at approximately 0.27 with the transition between the two regimes occurring at $De \sim 1$. This is in contrast to the low-strain asymptotic results that show peaks in $I_{3/1}$ at a Deborah number $\sim$2.

C. Simulation results

In this section, the Pompom model is explored in LAOS with the Pompom equations solved using the numerical techniques detailed in Sec. III.

In Figs. 3 and 4, the asymptote of $I_{3/1}$ shows one peak that occurs at higher Deborah numbers with increased ratio. This is in contrast to results shown in Hyun *et al.* (2013), where a secondary peak is observed at higher Deborah numbers. The asymptotes are an analytical solution of the Pompom model and are therefore the correct solutions in the limit of low-strain amplitude. We believe the secondary peak observed by Hyun *et al.* (2013) is a numerical artifact associated with how the Fourier transform was taken. In Fig. 5, a one mode Pompom model is simulated for a constant strain amplitude of $\gamma_0 = 0.01$ as a function of Deborah number. The Pompom parameters chosen are $G = 1$ Pa, $\tau_b = 1$ s, $q = 20$, and $r = 10$. The simulation is repeated with different choices (120 cycles, 480 cycles, and 1920 cycles) of sampling used to calculate the Fourier transform. It can be seen in the figure that when the Deborah number is equal to the number cycles sampled there is a peak in the noise (calculated from the second harmonic, which is mathematically zero) which can be seen as a secondary hump in the simulated value of $I_{3/1}$. This phenomenon can also be seen in Hyun *et al.* (2013) in Fig. 3. The quoted number of periods sampled is 32, and this coincides with the secondary peak in the relative third harmonic. It is clear that care must be taken when performing the numerical transform and the

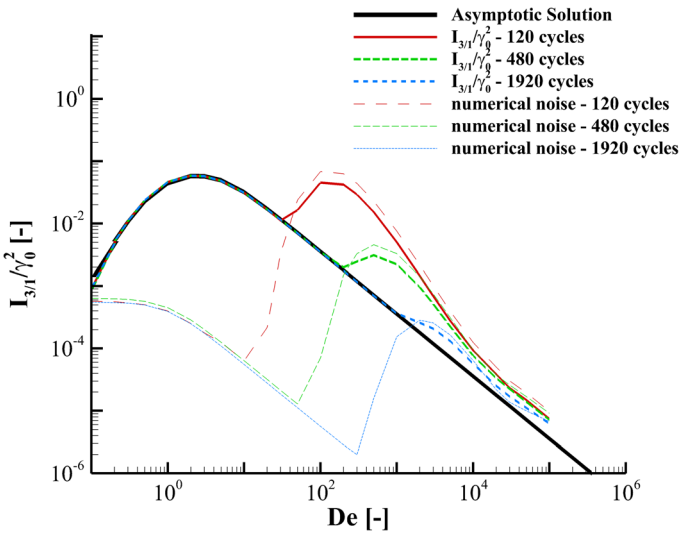

FIG. 5. The relative third harmonic $I_{3/1}$ plotted as a function of Deborah number for a one mode Pompom model with parameters $G = 1$ Pa, $\tau_b = 1$ s, $q = 20$, and $r = 10$, with a strain amplitude of 0.01 used for the simulations. The different lines show how the Fourier transform noise is affected by the number of cycles sampled.

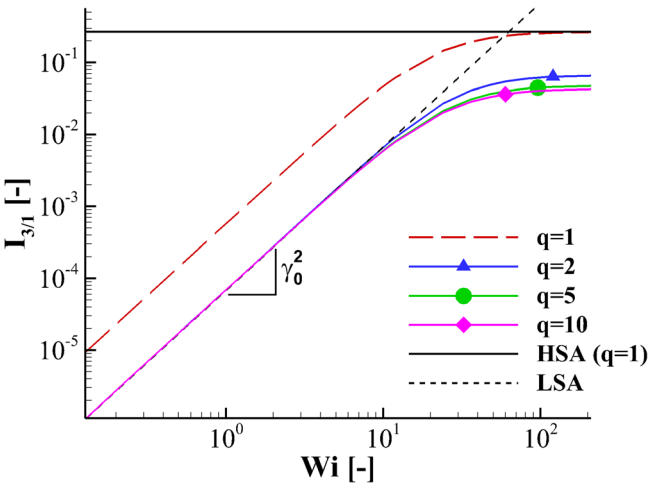

FIG. 6. The relative third harmonic $I_{3/1}$ plotted as a function of Weissenberg number for a one mode Pompom model with variations in branching priority, q. The other Pompom parameters are $G = 1000\,\text{Pa}$, $\tau_b = 10\,\text{s}$, and $r = 4$ giving a Deborah number, $De = 12$.

theoretical results in this paper have been sampled appropriately and the noise has been checked to ensure that it does not contribute to any rheological stress responses.

Experimentally, this effect will not be significant in this work due to the polydispersity of the samples. The polydispersity implies that there is a range of relaxation times and thus any effect of sample size will be averaged out over this distribution of characteristic times and subsequently reduced in significance.

Both theoretically and experimentally, this effect is also more pronounced at low-strain amplitudes. As the strain amplitude increases, the stress signal is increased significantly above the noise levels of the Fourier transform.

In Fig. 6, a one mode Pompom model is compared in LAOS for $De = 12$ and a range of branching priorities, $q = 1$, 2, 5, and 10. The solution agrees with the low-strain asymptote for Weissenberg numbers in the range $1 < W_i < 10$, and for the case $q = 1$ the high strain asymptote agrees with the solution for $W_i > 100$. The solution deviates from the low-strain asymptote at around a $W_i \sim 10$, at which point small differences can be seen for the various choices of q, for cases with $q > 1$.

In Fig. 7, a plot of $I_{3/1}$ is shown for various ratios of orientation and stretch relaxation time, $r = 1$, 2, 4, and 8, and constant branching priority, $q = 5$. For $r > 1$, the linear response superimposes onto the low-strain asymptote. For the case of $r = 1$, the leading order terms given in Eqs. (4.6) and (4.7) are zero so that $I_{3/1}$ is of order γ_0^4 and not γ_0^2. Comparing Figs. 6 and 7, it can be seen that the predominant Pompom parameter that controls the stress response in LAOS is the stretch relaxation time, τ_s.

In Fig. 8, the real and imaginary parts of the absolute value of the third harmonic, $I_{3/1}$, are plotted as a function of Weissenberg number for fixed Deborah number of $De = 12$, for various choices of branching priority, q, and ratio of orientation and stretch relaxation time, r. The linear Pompom parameters are chosen as $G = 1000\,\text{Pa}$ and $\tau_b = 10\,\text{s}$. The imaginary and real parts of $I_{3/1}$ are denoted as $I'_{3/1}$ and $I''_{3/1}$, respectively.

In Fig. 8 (left), the real and imaginary parts of $I_{3/1}$ are plotted for various choices of branching priority, q, and a fixed ratio, $r = 4$. For $q > 1$, there is only a small effect on the values of $I'_{3/1}$ and $I''_{3/1}$ with changing q. For $q = 1$, $I'_{3/1}$ is considerably larger than for the case of $q > 1$ and also for $q = 1$, $I''_{3/1}$ is positive as opposed to negative for the case $q > 1$.

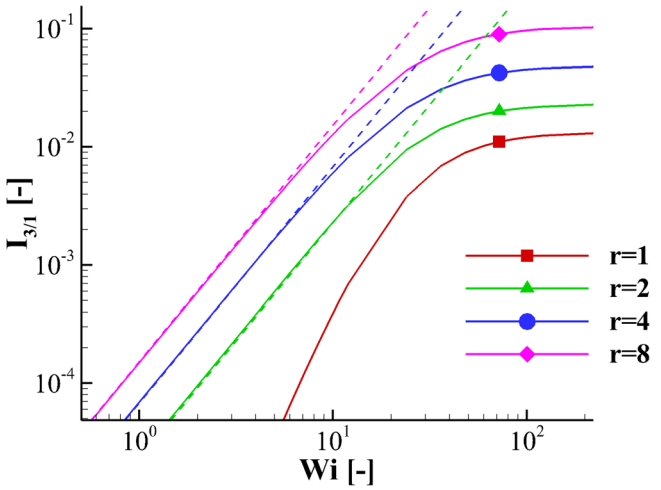

FIG. 7. The relative third harmonic $I_{3/1}$ plotted as a function of Weissenberg number for a one mode Pompom model with variations in the ratio of orientation and stretch relaxation times, r. The dashed lines represent the low-strain asymptotic solution and the simulation was performed at a fixed Deborah number of $De = 12$. The other Pompom parameters are $G = 1000\,\text{Pa}$, $\tau_b = 10\,\text{s}$, and $q = 5$.

As discussed above, the limit $q = 1$ is unphysical at high Weissenberg numbers as it neglects chain stretch, which occurs even for linear polymers at rates higher than the inverse chain Rouse time.

On the right of Fig. 8, the ratio of orientation and stretch relation times, r, is varied with a fixed branching parameter, $q = 5$. The figure shows the results for a fixed Deborah number of, $De = 12$, as a function of Weissenberg number. Again it can be seen that varying τ_s and hence r has a much bigger effect on $I'_{3/1}$ and $I''_{3/1}$ than the branching priority, q.

Studying the real and imaginary parts of $I_{3/1}$ provides a deeper insight into how a constitutive equation performs in LAOS, compared to the absolute value of $I_{3/1}$, since such quantities as the phase shift (of the nth harmonic) are calculated from I'_n and I''_n. In Sec. V, the principles discussed here are used to compare simulations of multimode Pompom constitutive model to experimental results of various polyethylenes.

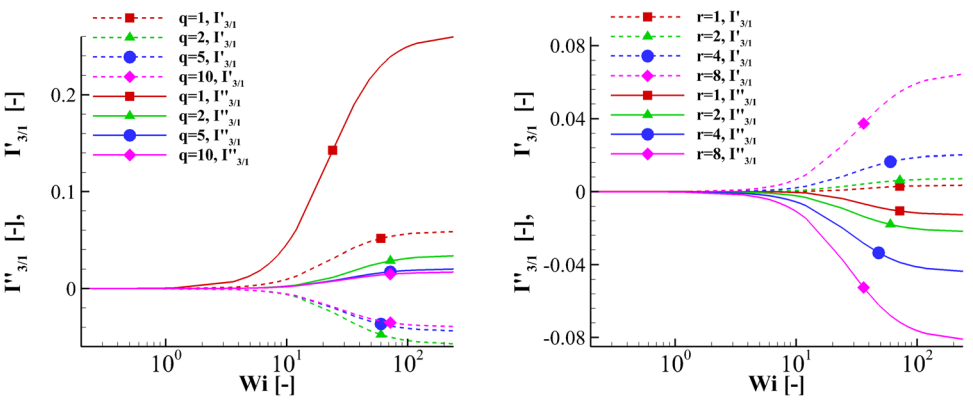

FIG. 8. The real and imaginary parts of the relative third harmonic, $I_{3/1}$, plotted against Weissenberg number for various choices of branching priority, q, (left) and the ratio of orientation and stretch relaxation times, r (right), both with $De = 12$.

V. EXPERIMENTAL RESULTS

In this study, we compare the results of three polyethylenes made from two different synthesis routes. We consider two branched HDPEs and an LDPE. The LDPE 1840H is produced by high pressure, high temperature free radical polymerisation, whereas the two HDPEs, HDB3 and HDB6, in this study are produced by metallocene catalyzed polymerisation, which is produced at relatively lower pressures and temperatures compared to that for the polymerisation of LDPE. Further details of these practices can be found in, for example Peacock (2000). These materials have been investigated and well characterized in previous studies, e.g., Costeux *et al.* (2002), Das *et al.* (2006), Hassell *et al.* (2008), and Hoyle *et al.* (2009, 2013).

A. Experimental and materials

The LAOS experiments were performed on a strain-controlled ARES rotational rheometer (Advanced Rheometric Expansion System, TA Instruments) using a 13 mm parallel plate geometry, with a gap of around 1 mm. The temperature was controlled through the use of the convection oven of the ARES, with heated nitrogen being flushed to achieve the desired temperature and avoid degradation. During the LAOS experiments, a temperature of 150 °C was used for 1840H, and 155 °C for HDB3 and HDB6. All the samples were previously prepared on a heated press under vacuum which ensured samples were free of trapped air bubbles and stress. For the frequencies of 0.2 Hz ($1.26\,\mathrm{rad\cdot s^{-1}}$) and 2 Hz ($12.6\,\mathrm{rad\cdot s^{-1}}$), eleven strain amplitudes between 0.1 and 1 (10% and 100% strain) equally spaced on a log-scale were used. For the lower frequency (0.02 Hz, $0.126\,\mathrm{rad\cdot s^{-1}}$), only six strains (also equally spaced) were used due to possible thermal degradation derived from the extended duration of the measurement. The apparent strain amplitudes were shifted to account for the use of a parallel plate, which does not provide homogeneous shear [cf. Wilhelm *et al.* (1999); Wagner *et al.* (2011)]. Adopting the results of Wagner *et al.* (2011), we shift the apparent strain amplitude to the true strain amplitude by a factor, $\sqrt{\frac{2}{3}}$.

For the analysis of the LAOS data, the FTR framework was used [van Dusschoten and Wilhelm (2001); Wilhelm (2002); Neidhöfer *et al.* (2003)]. The raw strain and torque data were collected directly from the ARES and externally digitized. The quantities obtained from Fourier analysis of the raw torque signal were the relative intensities of the higher harmonics $I_{n/1}$, and the relative phase differences Φ_n, as explained by Neidhöfer *et al.* (2003).

Rheological measurements of the materials in both small amplitude oscillatory and transient shear and uniaxial extensional flow were performed using a strain-controlled ARES rheometer advanced rheometric expansion system (Rheometric Scientific) with a force-rebalanced transducer (2 K-FRT). The specimens were compression moulded at 170–190 °C with the dimensions corrected for the thermal expansion. The rheological tests were repeated to assess the thermal stability and showed that no detectable molecular structure changes took place during the experiments.

SAOS tests were carried out using 10 mm parallel plates, while transient shear tests were carried out using various cone and plate geometries with cone angles between 2° and 10° and a diameter of 10 mm. Frequency sweeps were performed at a range of temperatures and the data shifted to the same temperature as the nonlinear rheology using WLF theory [Ferry (1961)].

The nonlinear elongational flow behavior was characterized using the uniaxial stretching device SER (Sentmanat elongational rheometer, Xpansion instruments [Sentmanat (2004)]) attached to the ARES rheometer. Different Hencky strain-rates between

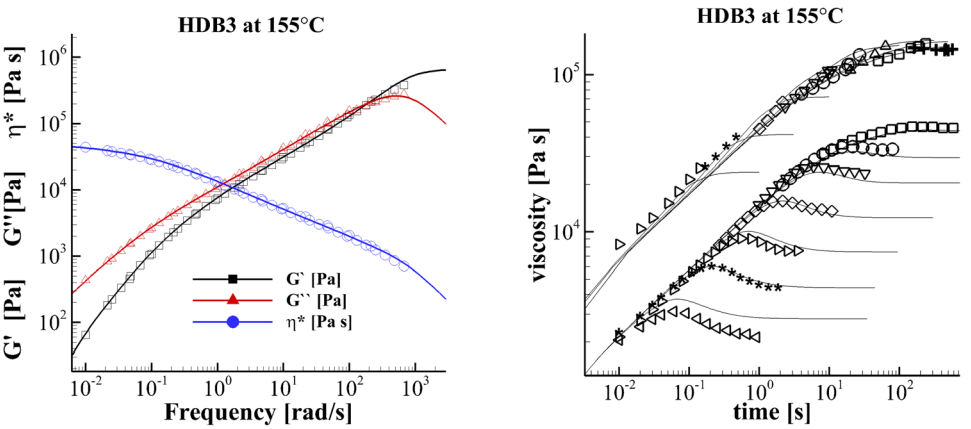

FIG. 9. A comparison between theory fitted to oscillatory shear, transient shear, and transient uniaxial extension for HDB3. Left: The dynamic moduli and complex viscosity fitted to a linear Maxwell spectrum. Right: Transient shear and transient uniaxial extension data used to fit the nonlinear parameters (τ_s and q) of the Pompom model. Data symbols correspond to shear/extension rates given in Table II and the Pompom parameters for HDB3 are given in Table III.

$0.001\,s^{-1}$ and $10\,s^{-1}$ were applied to compression molded specimens with a width from 3 to 10 mm and a thickness of about 1 mm [cf., for example, Münstedt and Auhl (2005)].

From this we will discuss the rheological tests commonly used to characterize polymer melts and then fit the experimental data with Pompom parameters. All experimental data in this paper were provided to us through the microscale polymer processing project (μPP^2).[1]

We shall now compare the predictions of the multimode Pompom model fitted to extensional rheology with experimental measurements for three materials, namely, the HDPEs; HDB3 and HDB6, and the LDPE, 1840H [Auhl *et al.* (2011)]. The Pompom model fitted to the experimental linear and non-linear rheology can be seen in Figs. 9–11 for HDB3, HDB6 and 1840H, respectively. All three materials have similar zero shear viscosities, of around 50 kPa.s, details of which and other material parameters can be found in Table I and the Pompom parameters used here can be found in the Appendix.

The linear and nonlinear Pompom parameters were fitted to data using *REPTATE* software (Ramirez and Likhtman[2]). This software provides an automated fitting tool which uses the downhill simplex method and searches for the minimum error between experimental data points and theory.

The multimode Pompom model described in Sec. II contains four parameters per mode. The linear Maxwell parameters are fitted to the dynamic moduli obtained from oscillatory shear measurements and as a further check the Maxwell parameters are then checked against the same data in the form of the complex viscosity. Frequency sweeps were performed at various temperatures and then are used to create a master curve using time-temperature superposition theory with two parameters [Ferry (1961)].

The nonlinear Pompom parameters, τ_{s_i} and q_i, are fitted using the protocol set out by Inkson *et al.* (1999). The authors suggest physical constraints on the choice of nonlinear Pompom parameters (τ_{s_i}, q_i). Namely, that the priority of branching must increase

[1]http://www.irc.leeds.ac.uk/mupp2/
[2]Ramirez, J., and A. E. Likhtman, Reptate: Rheology of entangled polymers, toolkit for analysis of theory and experiment, 2007, http://www.reptate.com.

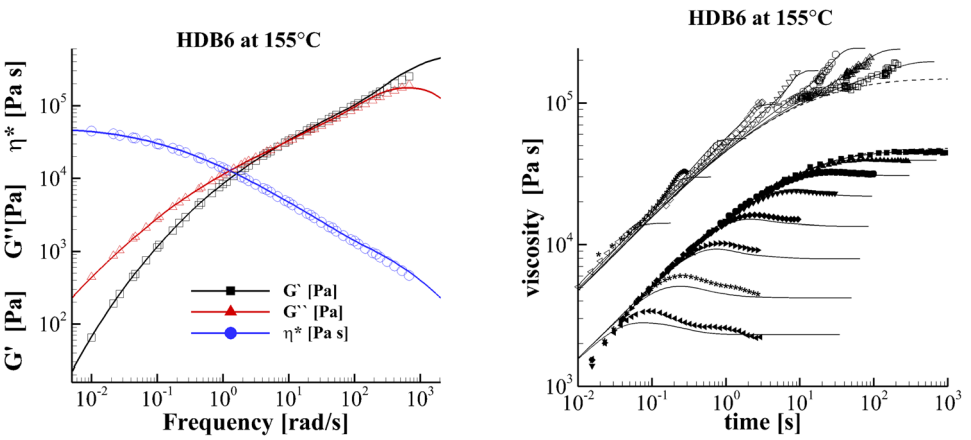

FIG. 10. A comparison between theory fitted to oscillatory shear, transient shear, and transient uniaxial extension for HDB6. Left: The dynamic moduli and complex viscosity fitted to a linear Maxwell spectrum. Right: Transient shear and transient uniaxial extension data used to fit the nonlinear parameters (τ_s and q) of the Pompom model. Data symbols correspond to shear/extension rates given in Table II and the Pompom parameters for HDB6 are given in Table IV.

toward the center of a molecule, i.e., the q_i is an increasing function in τ_{b_i} and that the ratio of relaxation times, $r_i = (\tau_b/\tau_s)$, is proportional to the number of entanglements in the backbone section. Although the number of entanglements is unknown the limit of $r_i = 1$ implies an unentangled backbone section. Inkson *et al.* (1999) also suggests that $\tau_{b_{i-1}} < \tau_{s_i}$, however, this rule is not strictly adhered to and in the interests of improving the fit between experimental data and theory the relaxation time ratios are varied in the range, $1 < r_i < 10$.

The nonlinear parameters are fitted to the extensional data and then against shear predictions. The value of q_i is mainly determined from the estimated limiting value in extensional viscosity at large strains. However, the extensional data obtained from the SER never reach a steady state plateau as stretching experiments are prone to sample

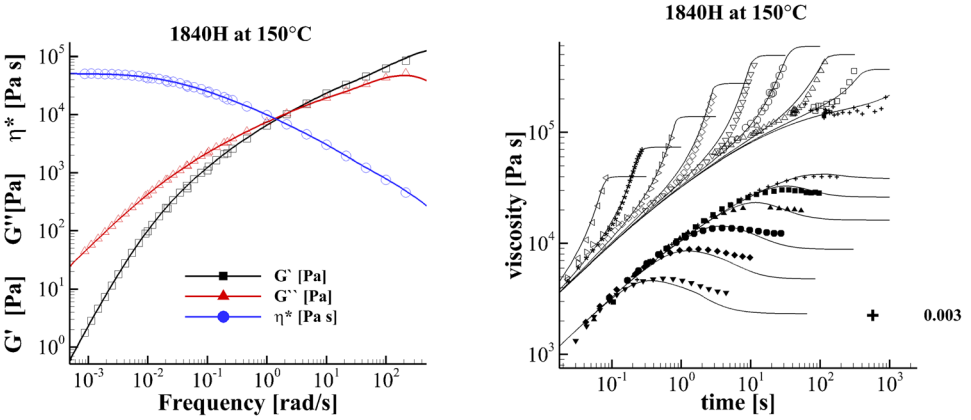

FIG. 11. A comparison between theory fitted to oscillatory shear, transient shear and transient uniaxial extension for 1840H. Left: The dynamic moduli and complex viscosity fitted to a linear Maxwell spectrum. Right: Transient shear and transient uniaxial extension data used to fit the nonlinear parameters (τ_s and q) of the Pompom model. Data symbols correspond to shear/extension rates given in Table II and the Pompom parameters for 1840H are given in Table V.

TABLE I. Material properties of polyethylenes investigated.

Sample	Code	M_W (kg/mol)	M_W/M_N (-)	T (°C)	η_0 (kPa s)	$\bar{\tau}_b$ (s)
Tubular	1840H	240	9	150	51	50
LCB-met.	HDB3	86	2.1	155	43	22.1
LCB-met.	HDB6	68	2.2	155	50	28

inhomogeneity and sample rupture [cf. Minoshima and White (1986a, 1986b); McKinley and Sridhar (2002); Aho *et al.* (2010a, 2010b)], and experiments are limited to Hencky strains less than four. This leaves an open question as to how to fit the Pompom theory to the data. We have chosen to fit the Pompom steady state plateau to equal the maximum SER data value reached before sample rupture.

This will enable us to consider the question: Can Pompom spectra with nonlinear parameters fitted to extensional data capture the behavior of branched materials in LAOS?

B. LAOS

In this section, a range of strain amplitudes typically larger than those used for SAOS are examined. Absolute strain amplitudes in the range $\gamma_0 = 0.1$ to $\gamma_0 = 1$ were accessible with the experimental technique used. Strain amplitudes beyond some critical point will depart from the low-strain asymptote which is proportional to the square of the strain amplitude, and tend to a plateau [e.g., Neidhöfer *et al.* (2003)]. This plateau is not reached in the experiments.

In the last section, it was shown that in a multimode Pompom constitutive model the number of modes with nonlinear parameters (i.e., modes with $q > 1$) affects the results for higher harmonics at small strain amplitudes. On a natural progression, one can ask if the number of nonlinear modes affect the LAOS results and how sensitive LAOS predictions are to the branching parameter, q? Another test for LAOS is to see if measurements can be used to distinguish between materials with differing levels of LCB.

Figure 12 shows a comparison between experiment and theory for each material for the three frequencies used in this study. Since each experiment is performed at a different Deborah number the value of $I_{3/1}$ is normalized by Deborah number for clarity and is plotted as a function of Weissenberg number. To calculate Deborah and Weissenberg numbers, the average relaxation time $\left(\bar{\tau} = \left(\Sigma_i G_i \tau_i^2 / \Sigma_i G_i \tau_i\right)\right)$ for each material was taken from Table I. The dotted lines represent the low-strain asymptotic solution derived in the last section and the solid lines are the numerical results. The experimental results follow the W_i^2 scaling predicted by the small strain asymptotic theory.

In general, the Pompom model (with parameters fitted to extensional rheology) is able to predict the experimental results with good accuracy, even departing from the W_i^2 behavior at the same point as experiments. The best results are for the intermediate frequency, 1.2 rad/s where experiment and theory agree well. The smallest and largest frequencies are modeled less precisely, with the Pompom parameterizations used here, over-predicting the experimental results.

As noted earlier, the imaginary and real parts, $I'_{3/1}$ and $I''_{3/1}$ respectively, contain phase information that does not appear in $I_{3/1}$. Figures 13–15 show the real and imaginary parts of the absolute third harmonic, $I_{3/1}$, plotted for varying Weissenberg numbers for HDB3, HDB6(a), and 1840H. Generally, the real part, $I''_{3/1}$, is larger and dominates the absolute modulus for each Deborah number. The initial quadratic behavior modeled by the low-strain asymptote of $I_{3/1}$ is seen in $I''_{3/1}$. In contrast, the imaginary part of the absolute

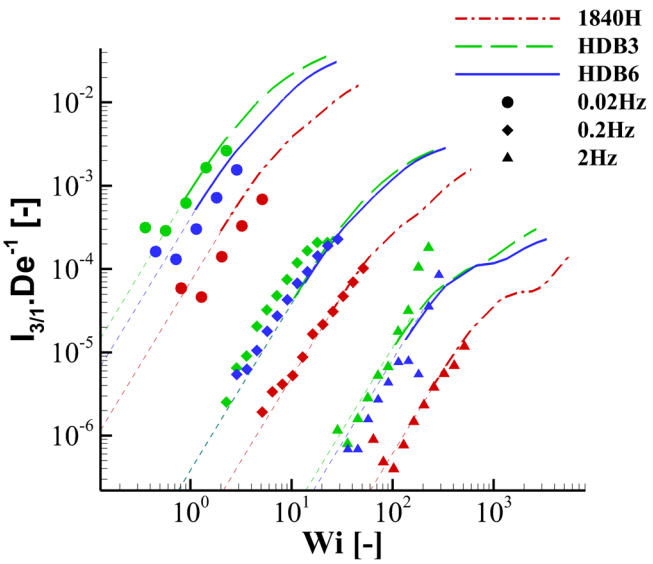

FIG. 12. A comparison between experiment and theory for each material for the three frequencies used in this study. Since each experiment is performed at a different Deborah number the value of $I_{3/1}$ is normalized by Deborah number for clarity and is plotted as a function of Weissenberg number. The dotted lines represent the low-strain asymptotic solution derived in the last section and the solid lines are the simulated results. Pompom parameters for each material are given in the appendix.

third harmonic, $I'_{3/1}$, is much smaller than $I''_{3/1}$ and tends to decrease and become negative. In each plot, the Pompom prediction is shown with a solid line in the experimental regime and a dotted line for Weissenberg numbers that were not experimentally available.

All the multimode Pompom spectra show a similar pattern of behavior with increasing W_i. The real part of $I_{3/1}$ typically grows quadratically with W_i before reaching a turning point, at which point $I''_{3/1}$ decreases and becomes negative. The imaginary part of $I_{3/1}$ is

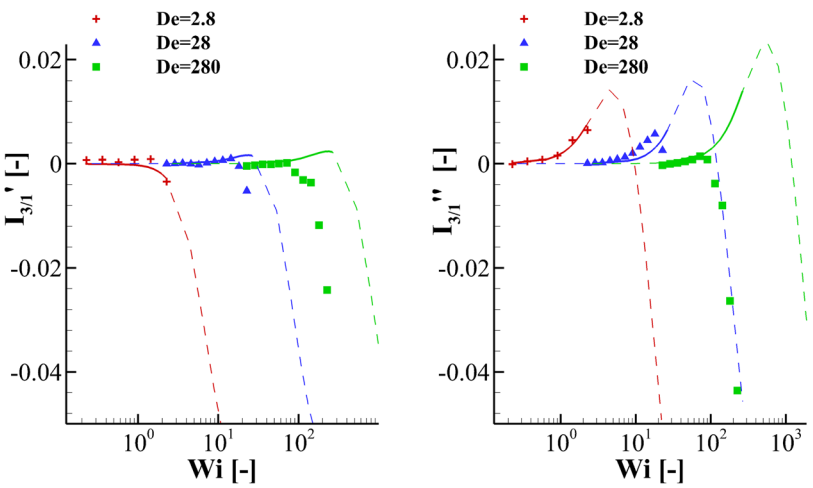

FIG. 13. A comparison between experiment and Pompom theory of the real (right) and imaginary (left) parts of $I_{3/1}$ for HDB3. The Pompom model has reasonable agreement with data with the biggest discrepancy occurring for the largest Deborah number, $De = 280$. The Pompom parameters for HDB3 are given in Table III.

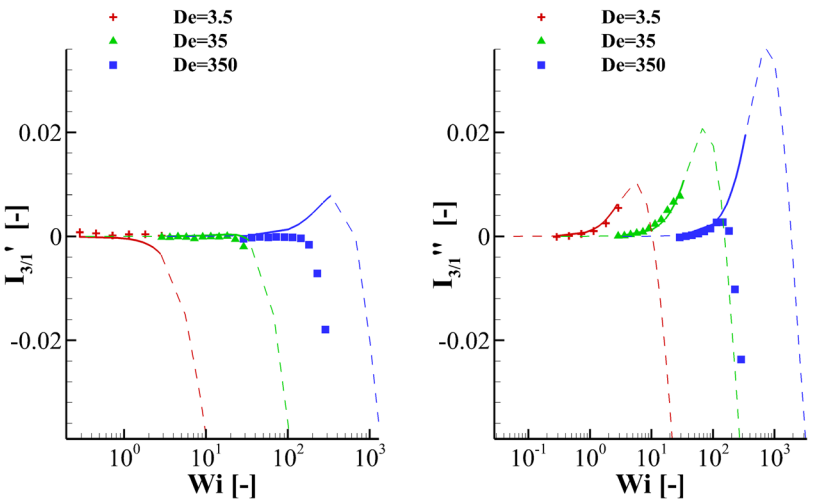

FIG. 14. A comparison between experiment and Pompom theory of the real (right) and imaginary (left) parts of $I_{3/1}$ for HDB6. The Pompom model has good agreement with data with the biggest discrepancy occurring for the largest Deborah number, $De = 350$. The Pompom parameters for HDB6 are given in Table IV.

much smaller than the real component but still grows negatively as the Weissenberg number is increased. For all three materials, the highest Deborah number plot of both $I'_{3/1}$ and $I''_{3/1}$ show maxima that are much higher than is observed experimentally.

For HDB3 $I'_{3/1}$ is modeled well for the lowest Deborah number ($De = 2.8$), but for the two higher Deborah numbers ($De = 28$, 280) the downturn occurs at a higher Weissenberg numbers for the model than in the experiments (cf. Fig. 13). The real component, $I''_{3/1}$, is predicted well for low Weissenberg numbers for all Deborah numbers, but the Pompom model predicts a maximum which is much higher than the data.

The results are similar for HDB6 (Fig. 14) with the first two Deborah ($De = 3.8$, 38) numbers being modeled well by the Pompom model, although slightly over-predicting the experimental data. For the highest Deborah number ($De = 380$), the Pompom model

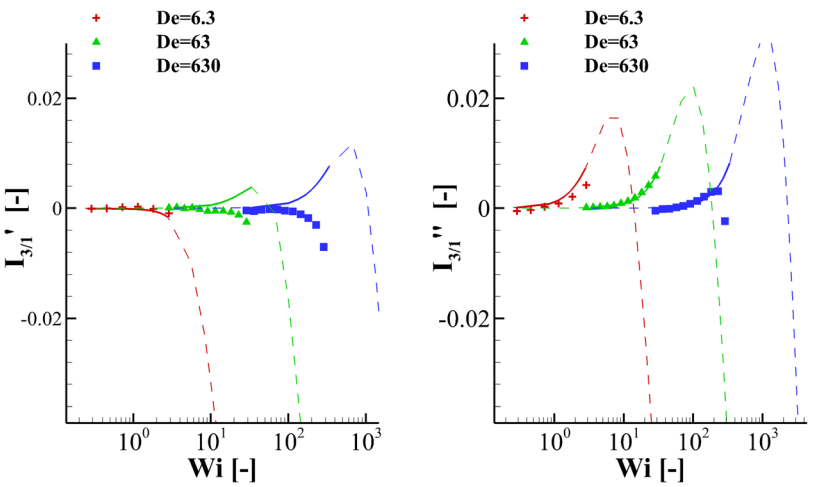

FIG. 15. A comparison between experiment and Pompom theory of the real (left) and imaginary (right) parts of $I_{3/1}$ for the LDPE 1840H. The Pompom model has good agreement with real data with the biggest discrepancy occurring for the imaginary component, $I'_{3/1}$, for the largest two Deborah numbers, $De = 63$ and $De = 630$. The Pompom parameters for 1840H are given in Table V.

TABLE II. The symbols used for transient shear and transient uniaxial extension plots in Figs. 9–11. Other strain-rates are specified in the plots.

Strain rate (s^{-1})	0.01	0.03	0.1	0.3	1.0	3.0	10	30
Symbol	□	△	○	▽	◇	▷	*	◁

generally over-predicts the experimental data and predicts a large maximum for both the real and imaginary components. No significant maximum is seen in the imaginary experimental data and the maximum observed in the real data is much smaller than the Pompom predictions.

For LDPE 1840H (Fig. 15), the lowest Deborah number experiment is predicted well by the Pompom model, however, $I''_{3/1}$ is still over-predicted. For the other two Deborah numbers, the Pompom model predicts a maximum in $I'_{3/1}$ which is not experimentally visible. For the largest Deborah number, the experiments find a downturn in $I''_{3/1}$ which is not captured by the Pompom model until much higher Weissenberg numbers.

Examining the real and imaginary components of the absolute third harmonic separately for all three materials gives greater insight into the performance of the Pompom equations in LAOS compared to looking at the absolute value alone. The imaginary component is much smaller than the real part and thus has little contribution to the absolute third harmonic thus studying this variable separately can show discrepancies not seen when studying the absolute third harmonic alone. Also both components become negative in the range of Weissenberg numbers accessible. The Pompom model captures the magnitude of the harmonic well but the prediction of the phase angle of the harmonic is poor. This can be seen, for example, in Figs. 12 and 14 in the largest Deborah number for the material HDB6, and for all the materials investigated here.

In general, the Pompom constitutive model with parameters fitted to extensional rheology captures the rheology of LAOS reasonably well. When discrepancies occur the Pompom model over-predicts experimental results. In the one mode Pompom model, we found that the value of $I_{3/1}$ showed a different rheological response for modes with a branching priority of $q = 1$ than for $q > 1$, in particular giving larger values of $I_{3/1}$. As noted earlier, a linear molecule would still exhibit chain stretch relaxation that is not modeled by the $q = 1$ Pompom model.

In fitting parameters to extensional data both the nonlinear Pompom parameters (τ_s and q) are fitted simultaneously and the fitting is most sensitive to the branching parameter, q. Using LAOS as a rheological technique can be used to ascertain the stretch relaxation time independently and provide a better understanding of material architecture. In particular, using the low-strain asymptotes allows an experimentally accessible method for investigating stretch relaxation time-scales.

VI. CONCLUSIONS

In this paper, the Pompom constitutive model was examined in LAOS to see if the model can successfully predict experimental results, and to determine the sensitivity of this experiment to the Pompom nonlinear parameters. In particular, can a Pompom parameter set that has been fitted to extensional data capture the behavior of the material in LAOS?

As this is a periodic flow it is convenient to use Fourier analysis to analyze the results. Since the first harmonic is dominated by the linear viscoelastic response, the most

sensitive measurements of nonlinearity come from the higher harmonics (which are zero for Oldroyd and UCM models). In this study, we focus our attention on the third harmonic Fourier coefficients, which are the largest nonlinear coefficients and hence most easily measured.

The Pompom parameters infer detail about molecular architecture and so by analyzing a one mode Pompom model it was possible to deduce which of the Pompom parameters are sensitive in LAOS. Of the two nonlinear Pompom parameters, the stretch relaxation time is the more dominant parameter, with the branching priority having only a minor effect on the stress response, for $q > 1$. For the Pompom model, a low-strain asymptotic solution was derived and from this it was shown that the absolute relative third harmonic, $I_{3/1}$, has a power law of 2, with respect to Weissenberg number. The low-strain asymptotes can be used to reduce computation time when simulating the full LAOS stress response and Fourier decomposition. The low-strain asymptotes are independent of branching parameter, q, and so provide a method for measuring τ_s alone.

The multimode Pompom model is compared to experimental data for three materials; two HDPEs HDB3, HDB6 and the LDPE 1840H. Experiments were performed at three frequencies (0.02, 0.2 and 2 Hz) and strain amplitudes ranging from $\gamma_0 = 0.1$ to $\gamma_0 = 1$. The Pompom parameters for each material were fitted to the dynamic moduli and extensional rheology and each spectrum shows a reasonable degree of accuracy in predicting $I_{3/1}$. Deviations away from the low-strain asymptote were hard to examine as the experimental data did not go far enough into the high strain regime. Overall, LAOS discriminated between the levels of LCB in the three samples. Analysis of the Pompom model shows this is probably not due to the number of branches but instead the number of branch-points, which is a subtle but important difference. This is reflected in the Pompom model with the sensitivity to the relaxation ratio, r, and not the branching priority, q.

To examine the accuracy of the Pompom model further, the variation of the real and imaginary parts of the relative third harmonic were examined with increasing strain amplitude (Weissenberg number). In general, the Pompom parameterizations agreed with experiments well for the two lower frequencies but large deviations occurred for the larger frequency. For the higher Weissenberg numbers both the real and imaginary components of $I_{3/1}$ showed a significant downturn, however, the Pompom model predicts a large peak and does not downturn until much higher Weissenberg numbers.

LAOS experiments provide a unique tool for analyzing branched polymer melts. The topic of this publication is characterizing LCB, but when trying to parameterize the Pompom model to flows such as transient extension the two nonlinear Pompom parameters are fitted for each mode simultaneously. This provides multiple fits all satisfying experimental rheology equally. In LAOS, the stress response is strongly dependent on only one nonlinear Pompom parameter and so could be used to determine this parameter independently. The low-strain asymptotes provide a powerful tool for this analysis as the experiments are easier to perform in this limit.

ACKNOWLEDGMENTS

The authors would like to thank Ewan Hemingway (Durham University) for useful discussions on numerical accuracy, and Gemma Blueitt for reading the work. The authors would also like to acknowledge the funding of the EPSRC-Microscale Polymer

Processing Grant No. GR/T11807/01. V.C.B. would like to thank the Technical University of Darmstadt and the German Research Foundation (DFG—Deutsche Forschungsgemeinschaft) for financial support.

APPENDIX: POMPOM PARAMETERS USED IN THIS STUDY

Tables III–V detail the Pompom parameters used in this study.

TABLE III. A list of Pompom parameters for material HDB3 used in this study. Linear Maxwell parameters are fitted to oscillatory shear and nonlinear parameters are fitted to transient shear and uniaxial flow.

	HDB3 at 155 °C, 12 modes			
Mode	G_i(Pa)	$\tau_{b,i}$(s)	$\tau_{b,i}/\tau_{s,i}$	q_i
1	422713	0.0016	—	1
2	116060	0.0043	—	1
3	62123.9	0.0118	—	1
4	30703.6	0.0323	—	1
5	16501.1	0.0882	—	1
6	9527.73	0.2409	—	1
7	5934.25	0.6579	—	1
8	3362.16	1.7970	2	1.3
9	1770.38	4.9081	9	1.4
10	688.780	13.405	9	1.5
11	147.668	36.613	9	1.8
12	64.4183	100.00	7	5

TABLE IV. A list of Pompom parameters for material HDB6 used in this study. Linear Maxwell parameters are fitted to oscillatory shear and nonlinear parameters are fitted to transient shear and uniaxial flow.

	HDB6 at 155 °C, 12 modes			
Mode, i	G_i(Pa)	$\tau_{b,i}$(s)	$\tau_{b,i}/\tau_{s,i}$	q_i
1	219226	0.0009	—	1
2	179387	0.0028	—	1
3	37873.9	0.0093	—	1
4	32981.4	0.0306	—	1
5	18896.9	0.1009	—	1
6	11820.4	0.3333	—	1
7	6053.40	1.1009	—	1
8	2767.03	3.6361	9	3
9	840.575	12.009	9	3
10	224.024	39.662	3	5
11	26.7746	130.99	2	8
12	1.94559	432.63	7	20

TABLE V. A list of Pompom parameters for materials 1840H used in this study. Linear Maxwell parameters are fitted to oscillatory shear and nonlinear parameters are fitted to transient shear and uniaxial flow.

	1840H at 155 °C, 12 modes			
Mode, i	G_i(Pa)	$\tau_{b,i}(s)$	$\tau_{b,i}/\tau_{s,i}$	q_i
1	64373.3	0.0032	—	1
2	37846.4	0.0100	—	1
3	13408.4	0.0316	1.3	4
4	14121.9	0.1000	4.7	5
5	7155.58	0.3162	5	5
6	4417.12	1.0000	5	6
7	2191.35	3.1622	5	7
8	1034.37	10.000	5	8
9	404.689	31.623	2.6	9
10	88.1892	100.00	2.6	14
11	7.91095	316.23	1	15
12	0.34016	1000.0	1	16

References

Aho, J., V. H. Rolon-Garrido, S. Syrjala, and M. H. Wagner, "Measurement technique and data analysis of extensional viscosity for polymer melts by Sentmanat extensional rheometer (SER)," Rheol. Acta, **49**(4), 359–370 (2010a).

Aho, J., V. H. Rolon-Garrido, S. Syrjala, and M. H. Wagner, "Extensional viscosity in uniaxial extension and contraction flow—Comparison of experimental methods and application of the molecular stress function model," J. Non-Newtonian Fluid Mech., **165**(5–6), 212–218 (2010b).

Auhl, D., D. M. Hoyle, D. Hassell, T. D. Lord, O. G. Harlen, M. R. Mackley, and T. C. B. McLeish, "Cross-slot extensional rheology and the steady state extensional response of long chain branched polymer melts," J. Rheol. **55**(4), 875–900 (2011).

Blackwell, R. J., O. G. Harlen, and T. C. B. McLeish, "Molecular drag-strain coupling in branched polymer melts," J. Rheol. **44**(1), 121–136 (2000).

Burden, R. L., and J. D. Faires, *Numerical Recipes* (Thomson Learning, Pacific Grove, CA, 2001).

Clemeur, N., R. P. G. Rutgers, and B. Debbaut, "On the evaluation of some differential formulations for the Pompom constitutive model," Rheol. Acta **42**, 217–231 (2003).

Costeux, S., P. Wood-Adams, and D. Beigzadeh, "Molecular structure of metallocene-catalyzed polyethylene: Rheologically relevant representation of branching architecture in single catalyst and blended systems," Macromolecules **35**(7), 2514–2528 (2002).

Das, C., N. J. Inkson, D. J. Read, and K. Kelmanson, "Computational linear rheology of general branch-on-branch polymers," J. Rheol., **50**(2), 207–234 (2006).

Debbaut, B., and H. Burhin, "Large amplitude oscillatory shear and Fourier-transform rheology for a high-density polyethylene: Experiments and numerical simulation," J. Rheol. **46**(5), 1155–1176 (2002).

Doi, M., and S. F. Edwards, *The Theory of Polymer Dynamics* (Oxford Science Publications, Oxford, 1986).

Ewoldt, R. H., A. E. Hosoi, and G. H. McKinley, "New measures for characterizing nonlinear viscoelasticity in large amplitude oscillatory shear," J. Rheol. **52**(6), 1427–1458 (2008).

Ewoldt, R. H., and G. H. McKinley, "On secondary loops in LAOS via self-intersection of Lissajous Bandwidth curves," Rheol. Acta **49**, 213–219 (2010).

Ferry, J. D., *Viscoelastic Properties of Polymers* (John Wiley and Sons Inc., New York, 1961).

Fleury, G., G. Schlatter, and R. Muller, "Non-linear rheology for long chain branching characterization, comparison of two methodologies: Fourier transform rheology and relaxation," Rheol. Acta **44**, 174–187 (2004).

Gabriel, C., J. Kaschta, and H. Münstedt, "Influence of molecular structure on rheological properties of polyethylenes," Rheol. Acta **37**, 7–20 (1998).

Graham, R. S., A. E. Likhtman, T. C. B. McLeish, and S. Milner, "Microscopic theory of linear, entangled polymer chains under rapid deformation including chain stretch and convective constraint release," J. Rheol. **47**(5), 1171–1200 (2003).

Graham, R. S., T. C. B. McLeish, and O. G. Harlen, "Using the Pompom equations to analyze melts in exponential shear," J. Rheol. **45**(1), 275–290 (2001).

Hassell, D. G., D. Auhl, T. C. B. McLeish, O. G. Harlen, and M. R. Mackley, "The effect of viscoelasticity on stress fields within polyethylene melt flow for a cross-slot and contraction-expansion slit geometry," Rheol. Acta **47**, 821–834 (2008).

Hoyle, D. M., "Constitutive modeling of branched polymer melts in non-linear response," Ph.D. thesis, University of Leeds, UK, 2010.

Hoyle, D. M., O. G. Harlen, D. Auhl, and T. C. B. McLeish, "Non-linear step strain of branched polymer melts," J. Rheol. **53**(4), 917–942 (2009).

Hoyle, D. M., Q. Huang, D. Auhl, D. Hassell, H. K. Rasmussen, A. L. Skov, O. G. Harlen, O. Hassager, and T. C. B. McLeish, "Transient overshoot extensional rheology of long-chain branched polyethylenes: Experimental and numerical comparisons between filament stretching and cross-slot flow," J. Rheol. **57**(1), 293–313 (2013).

Hyun, K., E. S. Baik, K. H. Ahn, S. J. Lee, M. Sugimoto, and K. Koyama, "Fourier-transform rheology under medium amplitude oscillatory shear for linear and branched polymer melts," J. Rheol. **51**(6), 1319–1342 (2007).

Hyun, K., K. H. Ahn, S. J. Lee, M. Sugimoto, and K. Koyama, "Degree of branching of polypropylene measured from Fourier-transform rheology," Rheol. Acta **46**, 123–129 (2006).

Hyun, K., and M. Wilhelm, "Establishing a new mechanical nonlinear coefficient Q from FT-Rheology: First investigation of entangled linear and comb polymer model system," Macromolecules **42**(1), 411–422 (2009).

Hyun, K., M. Wilhelm, C. O. Klein, K. Soo Cho, J. Gun Nam, H. Hyun Ahn, S. Jong Lee, R. H. Ewoldt, and G. H. McKinley, "A review of nonlinear oscillatory shear tests: Analysis and application of large amplitude oscillatory shear (LAOS)," Prog. Polymer Sci. **36**, 1697–1753 (2011).

Hyun, K., W. Kim, S. Park, and M. Wilhelm, "Numerical simulation results of the nonlinear coefficient Q from ft-rheology using a single mode pompom model," J. Rheol. **57**(1), 1–25 (2013).

Inkson, N. J., T. C. B. McLeish, O. G. Harlen, and D. J. Groves, "Predicting low density polyethylene melt rheology in elongational and shear flows with Pompom constitutive equations," J. Rheol. **43**(4), 873–896 (1999).

Kempf, M., D. Ahirwal, M. Cziep, and M. Wilhelm, "Synthesis and Linear and Nonlinear Melt Rheology of Well-Defined Comb Architectures of PS and PpMS with a Low and Controlled Degree of Long-Chain Branching," Macromolecules **46**, 4978–4994 (2013).

Lee, K., M. R. Mackley, T. C. B. McLeish, T. M. Nicholson, and O. G. Harlen, "Experimental observation and numerical simulation of transient stress fangs within flowing molten polyethylene," J. Rheol. **45**(6), 1261–1277 (2001).

Li, X., S. Q. Wang, and X. Wang, "Nonlinearity in large amplitude oscillatory shear (LAOS) of different viscoelastic materials," J. Rheol. **53**(5), 1255–1274 (2009).

Lohse, D. J., S. T. Milner, L. J. Fetters, M. Xenidou, N. Hadjichristidis, R. A. Mendelson, C. A. Garcia-Franco, and M. K. Lyon, "Well-defined, model long chain branched polyethylene. 2. Melt rheological behavior," Macromolecules **35**, 3066–3075 (2002).

MacSporran, W. C., and R. P. Spiers, "The dynamic performance of the Weissenberg rheogoniometer III. Large amplitude oscillatory shearing—harmonic analysis," Rheol. Acta **23**, 90–96 (1984).

Malmberg, A., C. Gabriel, T. Steffl, H. Münstedt, and B. Löfgren, "Long-chain branching in metallocene-catalyzed polyethylenes investigated by low oscillatory shear and uniaxial extensional rheometry," Macromolecules **35**, 1038–1048 (2002).

McKinley, G. H., and T. Sridhar, "Filament-stretching rheometry of complex fluids," Annu. Rev, Fluid Mech. **34**, 375–415 (2002).

McLeish, T. C. B., "Tube theory of entangled polymers," Adv. Phys. **51**, 1379–1527 (2002).

McLeish, T. C. B., and R. G. Larson, "Molecular constitutive equations for a class of branched polymers: The pompom polymer," J. Rheol. **42**(1), 81–110 (1998).

Minoshima, W., and J. L. White, "Instability phenomena in tubular film and melt spinning of rheologically characterised high density, low density and linear low density polyethylenes," J. Non-Newtonian Fluid Mech. **19**, 275–302 (1986a).

Minoshima, W., and J. L. White, "A comparative experimental study of the isothermal shear and elongational rheological properties of low density, high density and linear low density polyethylenes," J. Non-Newtonian Fluid Mech. **19**, 251–274 (1986b).

Münstedt, H., and D. Auhl, "Rheological measuring techniques and their relevance for the molecular characterization of polymers," J. Non-Newtonian Fluid Mech. **128**, 62–69 (2005).

Münstedt, H., S. Kurzbeck, and L. Egersdörfer, "Influence of molecular structure on rheological properties of polyethylenes," Rheol. Acta **37**, 21–29 (1998).

Neidhöfer, T., M. Wilhelm, and B. Debbaut, "Fourier-transform rheology experiments and finite-element simulations on linear polystyrene solutions," J. Rheol. **47**(6), 1351–1371 (2003).

Öttinger, H. C., "Thermodynamic admissibility of the Pompom model for branched polymers," Rheol. Acta **40**, 317–321 (2001).

Peacock, A. J., *Handbook of Polyethylene* (Marcel Dekker Inc., New York, 2000).

Press, W. H., S. A. Teukolsky, W. T. Vetterling, B. P. Flannery, and M. Metcalf, *Numerical Recipes: The Art of Scientific Computing* (Cambridge University, NY, 1996).

Schlatter, G., G. Fleury, and R. Muller, "Fourier transform rheology of branched polyethylene: Experiments and models for assessing the macromolecular architecture," Macromolecules, **38**, 6492–6503 (2005).

Sentmanat, M. L., "Miniature universal testing platform: From extensional melt rheology to solid-state deformation behavior," Rheol. Acta **43**(6), 657–669 (2004).

Trinkle, S., and C. Friedrich, "Van Gurp-Palmen plot: A way to characterize polydispersity of linear polymers," Rheol. Acta **40**, 322–328 (2001).

Trinkle, S., P. Walter, and C. Friedrich, "Van Gurp-Palmen plot II—Classification of long chain branched polymers by their topology," Rheol. Acta **41**, 103–113 (2002).

van Dusschoten, D., and M. Wilhelm, "Increased torque transducer sensitivity via oversampling," Rheol. Acta **40**(4), 395–399 (2001).

Vega, J. F., A. Santamaria, A. Muñoz Escalona, and P. Lafuente, "Small-amplitude oscillatory shear flow measurements as a tool to detect very low amounts of long chain branching in polyethylenes," Macromolecules **31**, 3639–3647 (1998).

Vega, J. F., M. Fernandez, A. Santamaria, A. Munoz-Escalona, and P. Lafuente, "Rheological criteria to characterize metallocene catalyzed polyethylenes," Macromolecules **200**, 2257–2268 (1999).

Venerus, D. C., "A critical evaluation of step strain flows of entangled linear polymer liquids," J. Rheol. **49**(1), 277–295 (2005).

Venerus, D. C., and R. Nair, "Stress relaxation dynamics of an entangled polystyrene solution following step strain flow," J. Rheol. **50**(1), 59–75 (2006).

Verbeeten, W. M. H., G. W. M. Peters, and F. P. T. Baaijens, "Differential constitutive equations for polymer melts: The extended Pompom model," J. Rheol. **45**(4), 823–843 (2001).

Vittorias, I., M. Parkinson, K. Klimke, B. Debbaut, and M. Wilhelm, "Detection and quantification of industrial polyethylene branching topologies via Fourier-transform rheology, NMR and simulation using the Pompom model," Rheol. Acta **46**, 321–340 (2007).

Vittorias, I., and M. Wilhelm, "Application FT rheology to industrial linear and branched polyethylene blends," Macromol. Mater. Eng. **292**, 935–948 (2007).

Wagner, M. H., and S. E. Stephenson, "The irreversibility assumption of network disentanglement in flowing polymer melts and its effects on elastic recoil predictions," J. Rheol. **23**(4), 489–504 (1979).

Wagner, M. H., V. H. Rolón Garrido, K. Hyun, and M. Wilhelm, "Analysis of medium amplitude oscillatory shear data of entangled linear and model comb polymers," J. Rheol. **55**(3), 495–516 (2011).

Wapperom, P., A. Leygue, and R. Keunings, "Numerical simulation of large amplitude oscillatory shear of a high-density polyethylene melt using the MSF model," J. Non-Newtonian Fluid Mech. **130**, 63–76 (2005).

Wilhelm, M., "Fourier-transform rheology," Macromol. Mater. Eng. **287**, 83–105 (2002).

Wilhelm, M., D. Maring, and H. W. Spiess, "Fourier-transform rheology," Rheol. Acta **37**, 399–405 (1998).

Wilhelm, M., P. Reinheimer, and M. Ortseifer, "High sensitivity Fourier-transform rheology," Rheol. Acta **38**, 349–356 (1999).

Wilhelm, M., P. Reinheimer, M. Ortseifer, T. Neidhöfer, and H. W. Spiess, "The crossover between linear and non-linear mechanical behaviour in polymer solutions as detected by Fourier-transform rheology," Rheol. Acta **39**, 241–246 (2000).

Wood-Adams, P. M., and J. M. Dealy, "Using rheological data to determine the branching level in metallocene polyethylenes," Macromolecules **33**, 7481–7488 (2000).

Wood-Adams, P. M., J. M. Dealy, A. W. deGroot, and O. D. Redwine, "Effect of molecular structure on the linear viscoelastic behavior of polyethylene," Macromolecules **33**, 7489–7499 (2000).